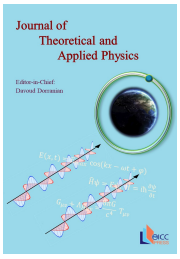

Volume 17, Issue 4, 172344 (1-11)

Journal of Theoretical and Applied Physics (JTAP)

https://dx.doi.org/10.57647/j.jtap.2023.1704.44

Exploring elastic mechanics and radiation shielding efficacy in neodymium(III)-enhanced zinc tellurite glasses: a theoretical and applied physics perspective

Hesham M. H. Zakaly [1,2,3]*, Y. S. Rammah [4], Shams A. M. Issa [1,5], N. Almousa [6], Adel M. El-Refaey [7], M. S. Shams [8]

[1]*Department of Physics, Faculty of Science, Al-Azhar University, Assiut Branch, Assiut, Egypt.*
[2]*Istinye University, Faculty of Engineering and Natural Sciences, Computer Engineering Department, Istanbul, Turkey.*
[3]*Institute of Physics and Technology, Ural Federal University, Yekaterinburg, Russia.*
[4]*Department of Physics, Faculty of Science, Menoufia University, Shebin El Koom, Egypt.*
[5]*Department of Physics, Faculty of Science, University of Tabuk, Tabuk, Saudi Arabia.*
[6]*Department of Physics, College of Science, Princess Nourah bint Abdulrahman University, Riyadh, Saudi Arabia.*
[7]*Department of Basic and Applied Science, Collage of Engineering and Technology, Arab Academy of Science, Technology and Maritime Transport, Smart Village, Giza, Egypt.*
[8]*Physics and Mathematical Engineering Department, Faculty of Electronic Engineering, Menoufia University, Menouf, Egypt.*

*__Corresponding author__: h.m.zakaly@gmail.com, h.m.zakaly@azhar.edu.eg

Received 14 April 2023; Accepted 6 June 2023; Published online 25 August 2023

Abstract:
The present work scrutinizes the radiation protection features and mechanical characteristics of neodymium zinc-tellurite of composition $[(TeO_2)_{70}\text{-}(ZnO)_{30}]_{1-x}\text{-}(Nd_2O_3)_x$: $x = 0-5$ mol% in steps of 1 (TZNd1 – 5). The Makishima–Mackenzie's model was adopted for the computation of the Poisson's ratio (PR) and elastic moduli. WinXcom and EXABCal software's were performed to evaluate the radiation shielding parameters and buildup factors, respectively of TZNd-glasses. Results revealed that the increasing of Nd_2O_3 concentration in TZNd-glasses from 1 to 5 mol% had a positive effect on their elastic parameters: Young's modulus increased from 53.13 to 54.81 GPa, bulk modulus changed from 31.95-33.65 GPa, and the PR varied from 0.222 to 0.228 for TZNd1 to TZNd5. There was a small increase in the Z/A as the Nd content increased, which leads to slight increase in TMSP of the particles. The mass attenuation coefficient (μ_m) increased in the order TZNd1 < TZNd2 < TZNd3 < TZNd4 < TZNd5. The maximum value of LAC obtained at 15 keV were 246, 249, 253, 257, and 260 cm^{-1} for TZNd1, TZNd2, TZNd3, TZNd4, and TZNd5, respectively. The HVT varies inversely with the linear attenuation coefficient. Throughout the considered energy spectrum the range of Z_{eff} for the glasses varied from $22.65-40.22$, $22.64-40.25$, $22.64-40.29$, $22.63-40.32$, and $22.63-40.36$ for TZNd1, TZNd2, TZNd3, TZNd4, and TZNd5, respectively. The values of fast neutron removal cross section Σ_R showed a steady increase as the partial densities of Nd and oxygen of the TZNd-glass systems increased. Generally, one can conclude that the additive of Nd_2O_3 to TeO_2-ZnO glasses leads to enhance their mechanical properties and increase their ability to absorb neutron and photon to apply in nuclear medicine applications.

Keywords: Mechanical features; Tellurite; Radiation protection; WinXcom; EXABCal code

1. Introduction

Scientific and technological advancements have persistently extended the utilization of Ionizing Radiation (IR) for human welfare, thus significantly escalating the number of radiation facilities globally [1]. Today, IR is widely employed in various sectors. These include the healthcare system for diagnostic and therapeutic procedures, and medical instru-

Table 1. Code, chemical composition, and density of the $[(TeO_2)_{70}\text{-}(ZnO)_{30}]_{1-x}\text{-}(Nd_2O_3)_x$: $x = 1$, 2, 3, 4 and 5 mol% glasses.

Sample code	Composition, (mol%)			Density,	Molar volume
	TeO_2	ZnO	Nd_2O_3	ρ (g/cm^3)$\pm$0.001	V_m (cm^3/mol)
TZNd1	69.3	29.7	1	5.390	25.628
TZNd2	68.6	29.4	2	5.437	25.775
TZNd3	67.9	29.1	3	5.507	25.811
TZNd4	67.2	28.8	4	5.570	25.879
TZNd5	66.5	28.5	5	5.606	26.070

ment sterilization; power industry for power generation; agriculture and food processing industries for crop enhancement and food preservation; scientific research for material characterization and isotope development, and environmental studies for pollution evaluation and geological structure delineation. Consequently, this broadening scope of IR applications has, over the years, sustained and occasionally elevated the radiation dose rate impacting both human beings and the environment from artificial IR sources [2, 3].

In light of the risks posed by unchecked radiation exposure, it becomes imperative to optimize all methods involving radiation of atomic and nuclear origin. From a radiation protection standpoint, optimization encompasses measures designed to minimize human and environmental radiation exposure to the lowest possible level. According to the International Commission on Radiation Protection (ICRP), safeguarding individuals from an external source incorporates three fundamental strategies: time reduction near radiation sources, space maximization between individuals and the sources, and using structural barriers to segregate people from the radiation source in all radiation installations [4]. Among these protective measures, shielding stands out as the most effective and practical method due to its minimal administrative oversight requirement.

Shielding involves the application of a barrier, often constructed of specific materials and designed to contain IR within a defined area, ensuring the radiation dose outside it remains at a safe level [5, 6]. The design of an appropriate shield necessitates a careful examination of radiation parameters, structural requirements of the source and facility, and the permissible dose rate outside the facility. Various parameters, depending on the type of IR, are used to gauge the shielding effectiveness of a material [7].

The potential of glass as a radiation protection barrier continues to gain recognition [8–13], primarily due to its advantages over many other radiation shielding materials [14, 15]. Glass shields are versatile and can be shaped into any geometry and size to contain and shield point radiation sources. Studies exploring the radiation shielding efficacy of numerous glass types with different structures and compositions have yielded promising results [16, 17]. Research into the radiation shielding parameters of different glasses is an active area of study. The flexible composition of glass, allowing the formation of new structures with superior shielding properties, is a key factor driving this research focus. Tellurite glasses, in particular, have exhibited excellent radiation shielding capacities for various IR classes due to their unique properties [18–22].

This study primarily aims to investigate the mechanical properties, proton and alpha-particle stopping power, range, photon shielding properties, and fast neutron removal cross-section of Nd_2O_3-doped tellurite-zinc (TZNd) glasses. We endeavor to enhance the existing data on tellurite-based glasses' shielding characteristics by examining the radiation (gamma-ray, neutron, proton, and α-particle) absorption capacity of neodymium-zinc-tellurite (TeO_2-ZnO-Nd_2O_3) glasses, referred to as TZNd-glasses, via WinXcom and EXABCal software. Additionally, we assess the mechanical characteristics of the TZNd-glasses.

2. Materials and theories

2.1 TZNd-glasses

Neodymium-zinc-tellurite glasses with composition $[(TeO_2)_{70}\text{-}(ZnO)_{30}]_{1-x}\text{-}(Nd_2O_3)_x$: $x = 0-5$ mol% in step increase of 1 were taken from Ref. [23]. These glasses codes are named TZNd-glasses. code of each glass sample, chemical compositions, and mass density are listed in Table 1.

Table 2. Coordination number per cation (n_f), crosslink density per cation (n_c), stretching force constant (F), packing density factor (V_i), and dissociation/bond energy per unit volume (G_i) of the oxides TeO_2, ZnO, and Nd_2O_3.

Oxide	n_f	n_c	F (N/m)	V_i (m^3/mol)	$G_i \times 10^6$ (KJ/m^3)
TeO_2	4	2	216	14.7	54
ZnO	6	4	219	8	49.9
Nd_2O_3	6	4	138.274	25.6	68.9

2.2 Mechanical characteristics

The Makishima-Mackenzie (Mak-Mac) model has been employed to examine the changes in oxide ratios of TZNd-glasses in response to variations in structure. This model incorporates several parameters, such as the stretching force constant (F), dissociation energy per unit volume (G_i), coordination number per cation (n_f), crosslink density per cation (n_c), and the packing density factor (V_i) of oxides in TZnd-glasses. These parameters are presented in Table 2 and are used to determine mechanical features such as Young's modulus (E_m), longitudinal modulus (L_m), hardness (H), shear modulus (G_m), Poisson's ratio (σm), and bulk modulus (K_m) of TZNd-glasses. The equations required to evaluate these mechanical features are outlined in Refs. [24, 25].

The Mak-Mac model is useful in analyzing the properties of TZNd-glasses, which are important in various applications. By examining the changes in oxide ratios of TZNd-glasses, this model provides insights into the structural changes that affect the mechanical properties of the glass. By evaluating parameters such as Young's modulus, hardness, and bulk modulus, researchers can better understand the performance of TZNd-glasses in specific applications. Overall, the Mak-Mac model provides a valuable framework for investigating the properties of TZNd-glasses and their potential applications.

2.3 Stopping power and projected range

When charged particles interact with a medium, they lose energy. This energy loss is commonly described in terms of Mass Stopping Power (MSP). For heavy ions, the MSP is typically calculated as the average energy loss per unit mass thickness, primarily due to Coulomb interactions between the ion and the orbital electrons of the medium.

The MSP of protons and α-particles in a glass medium can be estimated using parameters associated with both the charged particle and the glass material. An approximate expression has been developed to describe the relationship between these parameters and the MSP of the charged particle in the glass, as outlined in Refs. [26, 27].

Understanding MSP is crucial in various fields, including nuclear physics, materials science, and radiation therapy. The ability to accurately predict the energy loss of charged particles in a medium can provide insights into the behavior of ionizing radiation and its effects on materials. In medical applications, for example, MSP is an essential parameter in calculating the radiation dose delivered to cancerous tissues during proton therapy.

Overall, the characterization of MSP and its dependence on various factors is critical in predicting the behavior of charged particles in a medium and has significant implications in fields ranging from materials science to medicine.

$$\mathrm{MSP}_{glass} \propto \left(\frac{Z}{A}\right)_g z_{ion}^2 \left(\frac{m_{ion}}{T_{ion}}\right)^{k-1} \tag{1}$$

where, $(Z/A)_g$ is the number of electrons associated with a unit mass of the glass, z_{ion} the charge of the incident particle, m_{ion} and T_{ion} is the mass and kinetic energy of the traversing particle correspondingly, and $k \cong 1.8$ [26]. For a glass,

$$\left(\frac{Z}{A}\right)_g = \Sigma\left(\frac{\left(\frac{Z}{A}\right)_i^2}{\Sigma w_i \left(\frac{Z}{A}\right)_i}\right) \tag{2}$$

where w_i is the mass fraction of elements in the glass composition.

Also, the average thickness of a material which is enough to just stop a charged projectile is called the projected range (R) in the medium. Similar to the MSP, R may be expressed as [26, 27]:

$$\mathrm{R}_{glass} \propto \left(\frac{A}{\rho Z}\right)_g \frac{m_{ion}}{z_{ion}^2} \left(\frac{T_{ion}}{m_{ion}}\right)^k \tag{3}$$

To evaluate the Mass Stopping Power (MSP) and Range (R) of protons and α-particles in the glasses under investigation, the researchers utilized the SRIM-2013 software [28]. SRIM uses a quantum mechanical approach to calculate the interactions between charged particles and atoms in the TZNd-glass system, enabling the computation of MSP and R.

The use of SRIM-2013 is significant as it provides an accurate and reliable tool for predicting the behaviour of charged particles in materials. By utilizing a quantum mechanical approach, SRIM can account for various complex interactions between charged particles and atoms in the glass, such as electronic stopping and nuclear scattering. This approach allows for a more accurate estimation of MSP and R values than empirical methods that rely on experimental data alone.

Overall, the utilization of SRIM-2013 provides valuable insights into the behaviour of protons and α-particles in the TZNd-glass system. By computing MSP and R values, researchers can better understand the energy loss and penetration depth of charged particles in the glass. This information is essential in various fields, including radiation therapy and materials science, where the ability to predict the interaction of ionizing radiation with materials is critical for designing effective treatments and materials.

2.4 Photon attenuation quantities of TZNd-glasses

Numerous quantities may be used for explaining photon interaction features of the medium. Generally, the attenuation of a single energy beam of photons as they travel through a thin medium of thickness x (less than one free path) can be given by the Lambert-Beer expression:

$$I(x) = I_0 e^{-\sigma x} \tag{4}$$

where, $I(x)$ and I_0 is the photon energy flux after and before interacting with the absorber respectively. The $e^{-\sigma x}$ term in Equation (4) describes the degeneration in values of I_0 as a function of x. The parameter, σ depends on the characteristics of the absorbing medium. σ is referred to as the linear (μ) and mass (μ_m) attenuation coefficients of the absorber, when it's thickness, is stated in linear (cm), and mass thicknesses accordingly. For a given medium of density ρ, μ_m and μ are related as:

$$\mu_m = \frac{\mu}{m} \tag{5}$$

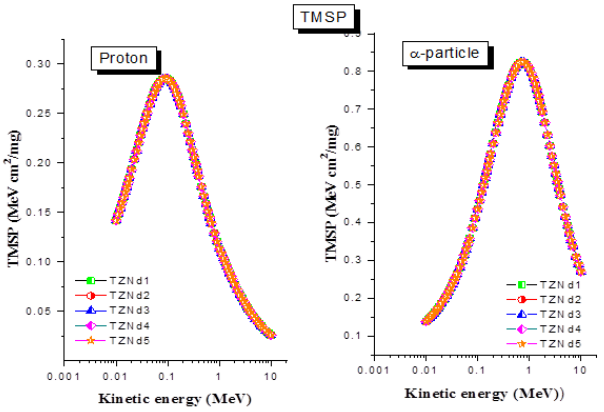

Figure 1. TMSP of proton and alpha-particle as a function of energy in TZNd-glasses.

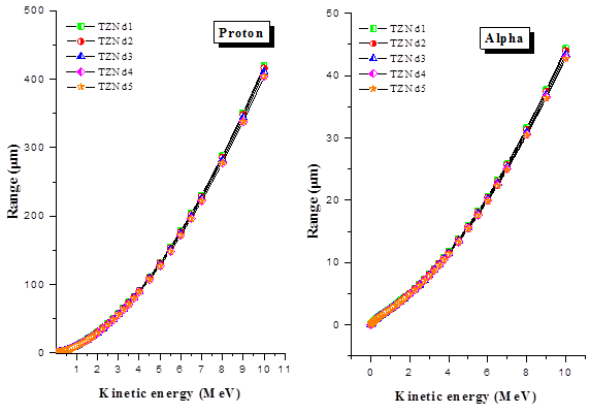

Figure 2. Projected range of proton and alpha-particle as a function of energy in TZNd-glasses.

The, μ_m and μ gives a measure of the fraction of incident photon flux that penetrates the shield without interacting. The μ_m of TZNd-glasses were evaluated in this work through WinXCom [29], while Equation (5) was used to estimate the μ.
The value of x in Equation (4) reduces I_0 by 50% is referred to as the HVT. The HVT is obtainable from μ thru the expression:

$$\mathrm{HVT} = \frac{\ln 2}{\mu} \tag{6}$$

The μ, μ_m, and HVT are critical parameters that are often used for relating the photon absorbing ability of diverse materials. HVT of the glasses in this study were evaluated through Equation (6).

2.5 Effective atomic number (Z_{eff}) of TZNd-glasses

When photon interaction with a compound or a chemical mixture is to be analyzed, the effective atomic number (Z_{eff}) comes to the fore. Z_{eff} characterizes the number of available electrons for photon interaction. This is important as most photon interaction procedures involve the electrons of the interacting compound/mixture. The Z_{eff} may be used to compare different media's relative photon absorption capacity.
Z_{eff} is related to μ_m based on the equation [30, 31].

$$Z_{eff} = \frac{\Sigma_i f_i A_i (\mu_m)_i}{\Sigma_i f_j \frac{A_i}{z_i} (\mu_m)_i} \tag{7}$$

The Z_{eff} of the glasses were calculated from the Auto-Z_{eff} software [32]. Values of Z_{eff} calculated from Equation (7) are consistent with those obtained from the software.

2.6 Photon buildup factors of TZNd-glasses

When scattered photons within the materials that emerged are considered, Equation (4) is usually corrected by multiplying it with factor B (photon buildup factor). The exposure (EBF) and energy absorption (EABF) buildup factors were estimated for the TZNd-glasses using the EXABCal software [33].

2.7 Removal cross section (Σ_R) of Neutron of TZNd-glasses

The ability of a glass medium to slow down fast neutrons is typically characterized by the fast neutron removal cross-section (Σ_R). In a similar manner to how the linear attenuation coefficient characterizes the interaction of photons with matter, (Σ_R) represents the removal of fast neutrons by the glass. The $(\Sigma_R)_g$ value for a given glass can be estimated using the addition rule, as outlined in Refs. [34, 35]:

$$(\Sigma_R)_g = \Sigma_i \rho_i \left(\frac{\Sigma_R}{\rho}\right)_i \tag{8}$$

Here, ρ_i and $(\Sigma_R/\rho)_i$ represent the density contribution and macroscopic removal cross-section of the elements present in the glass, respectively. The $(\Sigma_R/\rho)_i$ values can be obtained from Ref. [36].
Estimating $(\Sigma_R)_g$ is important for understanding the behavior of fast neutrons in glass materials. This information has implications in fields such as nuclear engineering, where the design of radiation shielding materials is critical for safety. The ability to predict the removal of fast neutrons by the glass is also important in developing new radiation detection materials and instruments.
Overall, the use of the addition rule to estimate $(\Sigma_R)_g$ provides a valuable tool for characterizing the slowing down of fast neutrons in glass materials. By considering the density contribution and macroscopic removal cross-section of each element present in the glass, researchers can better understand the behaviour of fast neutrons in the material and design effective radiation shielding and detection materials.

3. Results and discussion

3.1 Elastic moduli of TZNd-glasses

The Mak-Mac model is a widely accepted and reliable method for determining the elastic moduli of glass materials, which is based on the relationship between the total bond energy (G_t) and total ionic packing density (V_t) of the glasses. The model has been successfully applied in numerous studies to predict the mechanical properties of

Table 3. Total ionic packing density (V_t), total dissociation energy (G_t), Young's modulus (E_m), bulk modulus (K_m), shear modulus (G_m), longitudinal modulus (L_m), and Poisson's ratio (σ_m) based on Makishima-Mackenzie model of the TZNd1-TZNd5 glasses.

Sample code	V_t (m^3/mol)	$G_t \times 10^6$ (KJ/m^3)	E_m (GPa)	K_m (GPa)	G_m (GPa)	L_m (GPa)	H	σ_m
TZNd1	0.501	53.00	53.13	31.95	21.72	60.92	4.012	0.222
TZNd2	0.502	53.09	53.34	32.16	21.80	61.22	4.017	0.223
TZNd3	0.506	53.25	53.96	32.80	22.00	62.15	4.022	0.225
TZNd4	0.510	53.41	54.52	33.38	22.20	63.00	4.028	0.227
TZNd5	0.511	43.56	54.81	33.65	22.31	63.39	4.038	0.228

various glass systems. The total bond energy (G_t) and total ionic packing density (V_t) values for TZNd1-TZNd5 glasses were calculated using the method described in References and can be found in Table 3 [25, 26]. These values were employed in the Mak-Mac model to determine K_m, E_m, G_m, L_m, H, and σ_m, which are also listed in Table 3. The findings reveal that the (V_t) values exhibit a similar pattern to the molar volume parameter (V_m) displayed in Table 1. As a result of replacing Nd_2O_3 with TeO_2 and ZnO, the (G_t) values decreased from 53.00×10^6 (KJ/m^3) for TZNd1 to 43.56×10^6 (KJ/m^3) for TZNd5 glasses.

From Table 3, it can be observed that the minimum elastic coefficients were found for TZNd1 glass, while the maximum values were found for TZNd5 glass. This suggests that increasing Nd_2O_3 in the TZNd-glass compositions enhances their elastic moduli, hardness, and Poisson's ratio. This enhancement may be attributed to the formation of a higher number of bridging oxygen groups that increase the compactness of the glass structure, as outlined in Ref. [25][25]. Overall, the computation of G_t and V_t values for the TZNd1-TZNd5 glasses and their application in the Mak-Mac model provides a valuable tool for predicting the mechanical properties of these glasses. The observed trends in elastic coefficients and other mechanical properties provide insights into the structural changes in the glasses and have implications in various fields, including materials science and engineering.

3.2 Proton's and alpha-particles MSP and R in TZNd-glasses

Values TMSP of p and α in TZNd-glass samples as a function of kinetic energy T up to 10 MeV are shown in Figure 1. The result reveals a strong overlap between the TMSP of the glasses as Nd-concentration increased in the glasses. Nevertheless, a closer look at Figure 1 indicates that there is a slight increase in TMSP as Nd-molar concentration increased in the glass for both p and α and at each point in the energy spectrum considered. The observed trend is compatible with Equation (1). The (Z/A) of the glasses were 0.4367, 0.4368, 0.4368, 0.4369, and 0.4369 for TZNd1, TZNd2, TZNd3, TZNd4, and TZNd5, respectively. The almost constant value of Z/A ensured that their TMSP was almost equal as seen in Figure 1 for a particular particle. The slight increase in the Z/A as Nd-molar content en-

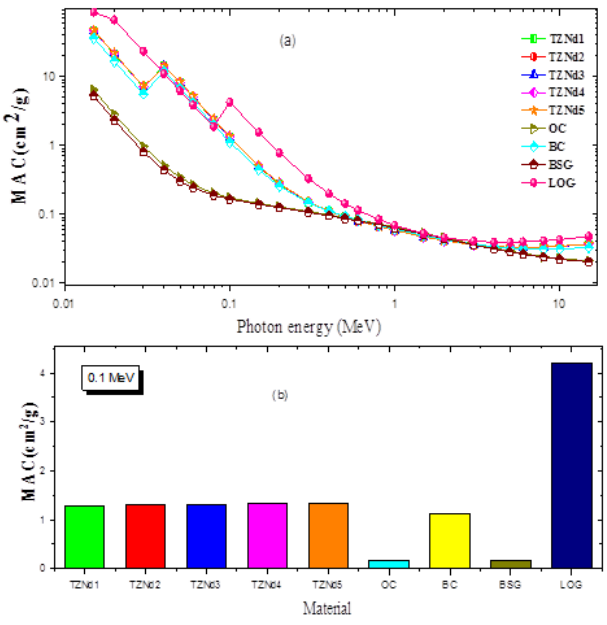

Figure 3. MAC of TZNd-glasses and other materials as a function of energy (a) and at 0.1 MeV (b).

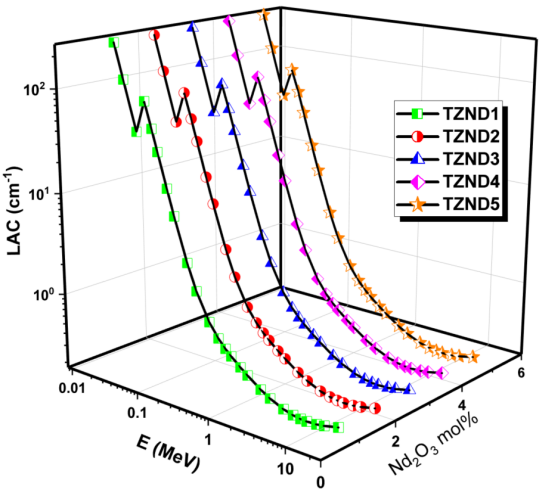

Figure 4. Variation of linear attenuation coefficients of TZNd-glasses with photon energy.

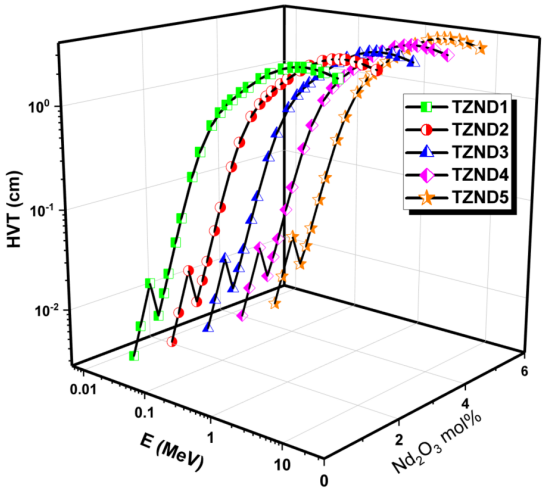

Figure 5. Variation of HVT of TZNd-glasses with photon energy.

hanced is responsible for the slight increase in TMSP of the particles. Also, at all values of T, the TMSP for α exceeds that of p. At the same T, the value of TMSP for p is about a third of that of α. This is consistent with the predictions of Equation (2). The maximum value of TMSP for p and α in all the glasses was obtained at 0.1 MeV and 0.6 MeV, respectively. The variation in the value of R of p and α in the TZNd-glasses concerning T is presented in Figure 2. The figure shows that R increases as T increases in all the glasses; this is consistent with the fact that $R_{glass} \propto (T_{ion})^k$ (Equation (3)). Also, R decreases as the concentration of Nd_2O_3 increases in the glass system. The trend in the projected range for each particle is in the order: of TZNd5 < TZNd4 < TZNd3 < TZNd2 < TZNd1. Accordingly, the particle's R varies directly with $A/\rho Z$ of the glasses. $A/\rho Z$ values for the TZNd-glass are 0.4248, 0.4211, 0.4157, 0.411, and 0.4082 cm^3/g for TZNd1, TZNd2, TZNd3, TZNd4, and TZNd5, individually. For all the glasses R of the proton exceed that of α at the same T. Due to the difference in masses, R for both p and α can be the same if they have the T per nucleon. This implies that the T of p would be 25% less than that of α for them to have equal R in the same glass material. From the results, the R of the α-particle was observed to be about 8.23% less than that of p at the same particle kinetic energy. The greater rest mass and electric charge of α explain this observation. The greater charge results in higher Coulomb potential, leading to higher force opposing the motion of the ion and hence stopping at a rather shorter range. Higher particle mass on its increases the collision probability with orbital electrons, thus giving rise to energy losses and continuous slowing down in the glass. Increasing the molar concentration of Nd_2O_3 increases the p and α absorbing capacity of TZNd-glasses.

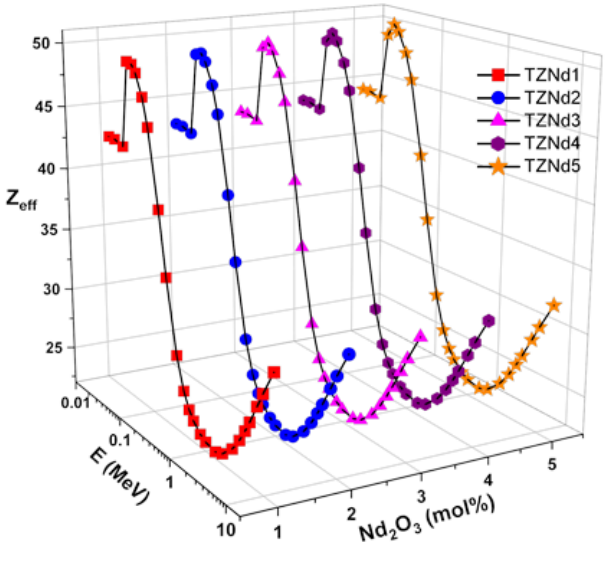

Figure 6. Changes in Z_{eff} of TZNd-glasses with photon energy.

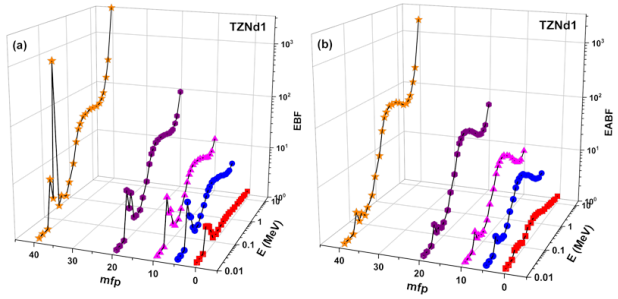

Figure 7. EBF (a) and EABF (b) of TZNd1 as a function of energy.

3.3 Photon shielding quantities

Mass attenuation coefficients (μ_m) of TZNd1, TZNd2, TZNd3, TZNd4, and TZNd5 as a function of photon energy from 15 keV to 15 MeV in comparison to those of barite concrete (BC), borosilicate glass (BSG), ordinary concrete (OC), and PbO-glass (LOG) [37] are presented in Figure 3a. Generally, the figure showed that μ_m decayed smoothly as photon energy decreases. The decay was discontinuous at 40 and 100 keV where peaks appeared. The sudden rise in μ_m at these two energies is attributed to the high photoelectric absorption of photons by K-shell electrons of Te and Pb, correspondingly. In all the TZNd-glass samples, the highest value of μ_m was gotten at 15 keV with corre-

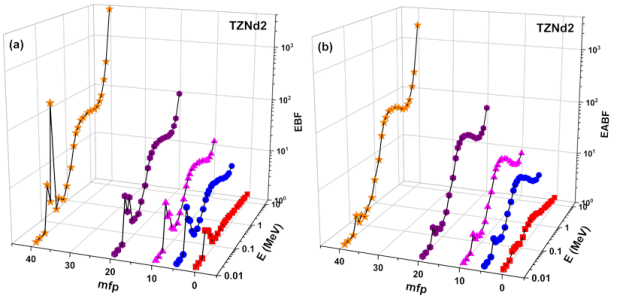

Figure 8. EBF (a) and EABF (b) of TZNd2 as a function of energy.

Table 4. Density, partial density, and Σ_R of TZNd1-TZNd5 glasses.

Glass	Density		Partial density	(g/cm^3)			Σ_R	(cm^{-1})		Total
Code	(g/cm^3)	Te	Zn	Nd	O	Te	Zn	Nd	O	(cm^{-1})
TZNd1	5.39	3.4863	0.7659	0.0571	1.0807	0.0467	0.014	0.0007	0.0438	0.1052
TZNd2	5.437	3.4677	0.7617	0.1136	1.0939	0.0465	0.0139	0.0014	0.0443	0.1061
TZNd3	5.507	3.4617	0.76	0.1735	1.1119	0.0464	0.0139	0.0022	0.045	0.1075
TZNd4	5.57	3.4517	0.7586	0.2312	1.1285	0.0463	0.0139	0.0029	0.0457	0.1087
TZNd5	5.606	3.4236	0.7523	0.291	1.1391	0.0459	0.0138	0.0036	0.0461	0.1094

sponding magnitudes of 45.58, 45.8, 46.0, 46.2, and 46.4 cm^2.g^{-1} for TZNd1, TZNd2, TZNd3, TZNd4, and TZNd5, respectively. The least value of μ_m was obtained at a photon energy of 6 MeV for all the TZNd-glasses included herein. The observed variations in the value of μ_m concerning energy can be attributed to the energy dependence of the cross sections of the various photon interaction procedures. The behaviours of these cross sections sum up that of μ_m. Generally, μ_m increase in the order at each energy as: TZNd1 < TZNd2 < TZNd3 < TZNd4 < TZNd5. This order is consistent with the mass density (ρ) of the glasses. Also, there is a direct relationship between the Nd_2O_3 content of the glasses and the mass density. The relative (μ_m) of the glasses were hence dictated by their ρ which in turn was dictated by the chemical content of the glasses. It may be concluded that the addition of Nd_2O_3 in the glass system thus improved the mass attenuation coefficients. Furthermore, comparing the mass attenuation of TZNd-glasses with those of BC, BSG PbO and LOG throughout the considered energy spectrum and at 0.1 MeV (Figure 3b), it can be seen that the TZNd-glasses have outstanding shielding concerning OC, BC and BSG. However, the (μ_m) of LOC was higher than those of the TZNd-glasses.

Figure 4 illustrates the changes in the linear attenuation coefficient (μ) of the TZNd-glasses in relation to photon energy. The behavior of μ among the TZNd-glasses is similar to that of the mass attenuation coefficient (MAC). However, variations in μ values are more pronounced due to the differences in glass density. The plots also show strong photoelectric absorption by the K-shell electrons. The highest linear attenuation coefficient values at 15 keV are: 246, 249, 253, 257, and 260 cm^{-1} for TZNd1, TZNd2, TZNd3, TZNd4, and TZNd5, respectively. HVT of TZNd-glasses concerning photon energy is shown in Figure 5. The HVT graph is the inverse of the linear and attenuation coefficients, therefore, the uppermost values of HVT were obtained for TZNd1. This is a result of its low density and LAC values. This also implies that photons move through the glass with relatively lower energy loss compared to the other TZNd-glass samples. The decrease in the HVT as Nd_2O_3 concentration increased to a maximum value of 5 mol% in TZNd-glasses was within 8%.

The variation of Z_{eff} for TZNd-glasses under study is depicted in Figure 6 in relation to photon energy. For the energy spectrum of interest, the range of Z_{eff} for the glasses varied from: $22.65-40.22$, $22.64-40.25$, $22.64-40.29$, $22.63-40.32$, and $22.63-40.36$ for TZNd1, TZNd2, TZNd3, TZNd4, and TZNd5, respectively. There was a peak at the K-absorption edge of Te. The characteristics of the Z_{eff} concerning energy is similar to that of the partial photon interaction modes dominating each energy. Hence, the value of Z_{eff} was maximum at the photon energy range where photoelectric absorption dominates and minimum where Compton interaction dictates photon interaction proceedings. The trend in the Z_{eff} is such that TZNd1 had the least Z_{eff} except at 1.5 MeV while TZNd5 had the highest. The range of the Z_{eff} is also dictated by the atomic number (Z) of the atomic species that make up the glasses' chemical structure. The least (maximum) Z_{eff} value is not less (more) than the least (maximum) Z value of the atoms in the composite [38–40]. The Z_{eff} the result shows that a higher effective atomic number implies a relatively higher photon absorbing capacity for the TZNd-glasses.

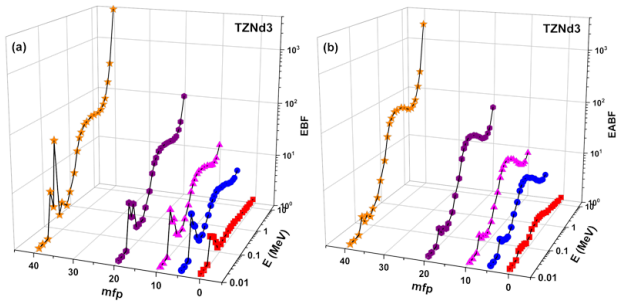

Figure 9. EBF (a) and EABF (b) of TZNd3 as a function of energy.

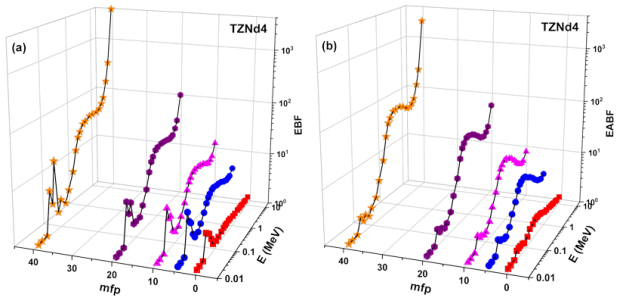

Figure 10. EBF (a) and EABF (b) of TZNd4 as a function of energy.

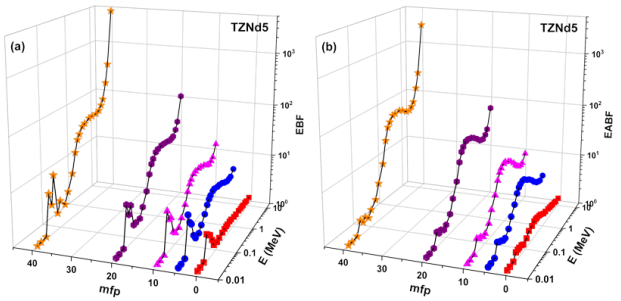

Figure 11. EBF (a) and EABF (b) of TZNd5 as a function of energy.

3.4 Exposure and energy absorption buildup factors (BUFs)

Figures 7-11 (a and b) present the energy-dependent attenuation buildup factors (EABF and EBF) for the five TZNd-glass systems at specified photon energies ranging from 0.15 MeV to 5 MeV and penetration depths of up to 40 mean free paths (MFP). The figures demonstrate that the variations in the buildup factors with photon energy follow a similar pattern for all glasses and penetration depths. Both EABF and EBF values are generally low at the lower end of the energy spectrum, except at absorption edges, and they increase with energy up to a peak for all glasses and depths. The higher buildup factors observed at elevated energies can be ascribed to Compton scattering and pair production interactions of the photons. The Compton scattering process reduces the energy of photons due to multiple scattering events, leading to an increased number of low-energy photons (i.e., buildup factors) within the glass medium.

The variation in the buildup factors with penetration depth is depicted in Figures 12 and 13. The buildup factors are lower at lower depths, but they increase quickly as the depth increases up to 40 MFP. This is because as the glass depth increases, photons suffer more collisions, leading to an increase in the number of low-energy photons building up in the glasses. Based on the energy dependence of the evaluated photon shielding parameters, it is clear that TZNd5 is a better photon absorber among the studied TZNd5 glasses. These findings have implications in various fields, including radiation protection and shielding design. By understanding the behaviour of photons in glass materials, researchers can better design and optimize radiation shielding materials to protect personnel and equipment from ionizing radiation.

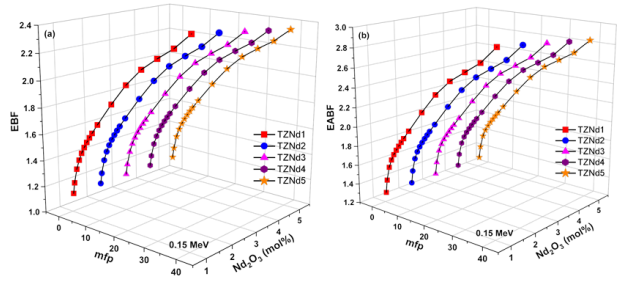

Figure 12. EBF (a) and EABF (b) as a function of depth at 0.15 MeV for TZNd-glasses.

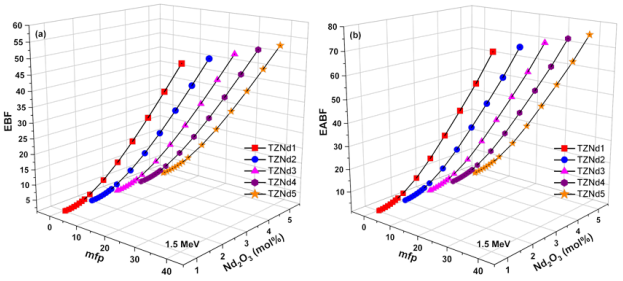

Figure 13. EBF (a) and EABF (b) as a function of depth at 1.5 MeV for TZNd-glasses.

3.5 Removal cross section (Σ_R) for fast neutrons

The computed partial density and Σ_R of the five TZNd5 glasses are shown in Table 4. The values of Σ_R indicate a steady increase as the partial densities of Nd and oxygen of the TZNd-glass systems increase. Based on the values of Σ_R, TZNd5 presents the best fast neutron shielding prowess. Based on the analysis of the photon and fast neutron interaction parameters, TZNd5 showed a superior capacity to absorb a photon and fast neutron among the TZNd glass samples.

4. Conclusion

This work examines the mechanical characteristics, proton, alpha, gamma-photon, and neutron protection features of neodymium zinc-tellurite of composition $[(TeO_2)_{70}\text{-}(ZnO)_{30}]_{1-x}\text{-}(Nd_2O_3)_x$: $x = 0-5$ mol% in steps of 1 (TZNd-glasses). Results confirmed that:

$\therefore$ Increasing Nd_2O_3 concentration in TZNd-glasses from 1 to 5 mol% had a positive effect on their elastic parameters: Young's modulus increased from 53.13 to 54.81 GPa, bulk modulus changed from $31.95-33.65$ GPa, shear modulus varied from 21.72 to 22.31 GPa, longitudinal modulus increased from $60.92-63.39$, and Poisson's ratio varied from 0.222 to 0.228 for TZNd1 to TZNd5.

$\therefore$ There was a slight increase in the Z/A as Nd-molar concentration increased, which leads to a slight increase in the TMSP of the particles. Also, for all particle kinetic energy, the TMSP for α was higher than that of p. $\therefore$ The increase in the molar concentration of Nd_2O_3 leads to an increase in the proton and alpha particle absorption capacity of TZNd-glasses.

$\therefore$ The order of the mass attenuation coefficient (μ_m) is: TZNd1 < TZNd2 < TZNd3 < TZNd4 < TZNd5.

$\therefore$ The peak value of LAC obtained at 15 keV was: 246, 249, 253, 257, and 260 cm^{-1} for TZNd1, TZNd2, TZNd3, TZNd4, and TZNd5, respectively.

$\therefore$ The HVT varies inversely to the linear attenuation coefficient, consequently, TZNd1 has the highest HVT.

$\therefore$ Within the investigated energy spectrum, Z_{eff} changes within the range: $22.65-40.22$, $22.64-40.25$, $22.64-40.29$, $22.63-40.32$, and $22.63-40.36$ for TZNd1, TZNd2, TZNd3, TZNd4, and TZNd5, respectively.

$\therefore$ The values of Σ_R showed a steady increase with the partial densities of Nd and oxygen of the TZNd-glass systems increased. TZNd5 thus presents the best fast neutron shielding prowess among the glasses.

The enhanced mechanical and radiation shielding properties of Nd_2O_3-doped tellurite-zinc glasses make them suitable candidates for applications in nuclear facilities, medical radiation therapy, and aerospace industries. However, further studies are needed to optimize the glass composition for specific applications and address potential limitations, such as the effect of prolonged radiation exposure on the glasses' structural stability and long-term performance. One can conclude that the additive of Nd_2O_3 to TeO_2-ZnO glasses enhances their mechanical properties and increases their ability to absorb neutrons and photons. Additionally, The TZNd5 with 5 mol% Nd_2O_3 concentration is a better photon shield than other investigated TZNd-glasses.

Acknowledgements:
The authors would like to express their gratitude to Princess Nourah bint Abdulrahman University Researchers Supporting Project (Grant No. PURSP2023R111), Princess Nourah bint Abdulrahman University, Riyadh, Saudi Arabia.

Conflict of interest statement:
The authors declare that they have no conflict of interest.

References

[1] W. Elshami, H. O. Tekin, S. A. M. Issa, M. M. Abuzaid, H. M. H. Zakaly, B. Issa, and A. Ene. "Impact of Eye and Breast Shielding on Organ Doses During Cervical Spine Radiography: Design and Validation of MIRD Computational Phantom. Front. Public Heal. 9, (2021)". *Frontiers in Public Health*, **9**:1, 2021.

[2] S. A. M. Issa, H. M. H. Zakaly, H. O. Tekin, H. A. Saudi, A. Badawi, M. Pyshkina, G. Susoy, A. I. Elazaka, and A. Ene. "Exploring the ftir, optical and nuclear radiation shielding properties of samarium-borate glass: A characterization through experimental and simulation methods". *Nanomaterials*, **11**:1713, 2021.

[3] A. El-Taher, H. M. H. Zakaly, M. Pyshkina, E. A. Allam, R. M. El-Sharkawy, M. E. Mahmoud, and M. A. E. Abdel-Rahman. "A comparative Study Between Fluka and Microshield Modeling Calculations to study the Radiation-Shielding of Nanoparticles and Plastic Waste composites". *Zeitschrift für Anorganische und Allgemeine Chemie*, **647**:1083, 2021.

[4] *The 2007 Recommendations of the International Commission on Radiological Protection*. ICRP publication 103, 2007.

[5] A. M. Abd-Elnaiem, H. A. Saudi, H. M. H. Zakaly, S. A. M. Issa, and M. Rashad. "The effect of composition and γ-irradiation on the Vickers hardness, structural and optical properties of xLiNbO3-25CaO-35PbO-(40-x) waste systems". *Ceramics International*, **47**:18751, 2021.

[6] A. Kavaz Yüksel, H. M. H. Zakaly, and A. Ene. "Evaluation of photon interaction parameters of some antioxidants for food irradiation applications". *Materials*, **15**:6376, 2022.

[7] H. M. H. Zakaly, H. A. Saudi, H. O. Tekin, M. Rashad, S. A. M. Issa, Y. S. Rammah, A. I. Elazaka, M. M. Hessien, and A. Ene. "Glass fabrication using ceramic and porcelain recycled waste and lithium niobate: physical, structural, optical and nuclear radiation attenuation properties". *Journal of Materials Research and Technology*, **15**:4074, 2021.

[8] B. Alshahrani, I. O. Olarinoye, C. Mutuwong, C. Sriwunkum, H. A. Yakout, H. O. Tekin, and M. S. Al-Buriahi. "Amorphous alloys with high Fe content for radiation shielding applications". *Radiation Physics and Chemistry*, **183**:109386, 2021.

[9] C. Bootjomchai, J. Laopaiboon, C. Yenchai, and R. Laopaiboon. "Gamma-ray shielding and structural properties of barium–bismuth–borosilicate glasses". *Radiation Physics and Chemistry*, **81**:785, 2012.

[10] A. A. A. Darwish, S. A. M. Issa, and M. M. El-Nahass. "Effect of gamma irradiation on structural, electrical and optical properties of nanostructure thin films of nickel phthalocyanine". *Synthetic Metals*, **215**:200, 2016.

[11] B. O. Elbashir, M. G. Dong, M. I. Sayyed, S. A. M. Issa, K. A. Matori, and M. H. M. Zaid. "Comparison of Monte Carlo simulation of gamma ray attenuation coefficients of amino acids with XCOM program and experimental data". *Results in Physics*, **9**:6, 2018.

[12] R. Boodaghi Malidarre, I. Akkurt, and H. M. H. Zakaly. "Investigation of Ag as chemical modifier in glassy SeTe chalcogenide alloy in terms of radiation shielding, optical, structural, and physical properties". *Radiation Physics and Chemistry*, **204**:110685, 2023.

[13] A.S. Abouhaswa, H. M. H. Zakaly, S. A. M. Issa, M. Pyshkina, R. El-Mallawany, and M. Y. A. Mostafa. "Lead borate glasses and synergistic impact of lanthanum oxide additive: optical and nuclear radiation shielding behaviors". *Journal of Materials Science: Materials in Electronics*, **31**:14494, 2020.

[14] H. M. H. Zakaly, M. A. M. Uosif, S. A. M. Issa, H. O. Tekin, H. Madkour, M. Tammam, A. El-Taher, G. A. Alharshan, and M. Y. A. Mostafa. "An extended assessment of natural radioactivity in the sediments of the mid-region of the Egyptian Red Sea coast". *Marine Pollution Bulletin*, **171**:112658, 2021.

[15] E. Ilik, E. Kavaz, G. Kilic, S. A. M. Issa, H. M. H. Zakaly, and H. O. Tekin. "A closer-look on Copper(II) oxide reinforced Calcium-Borate glasses: Fabrication and multiple experimental assessment on optical, structural, physical, and experimental neutron/gamma shielding properties". *Ceramics International*, **48**:6780, 2022.

[16] R. Boodaghi Malidarre, I. Akkurt, I. Ekmekci, H. M. H. Zakaly, and H. Mohammed. "The role of La2O3 rare earth (RE) material in the enhancement of the radiation shielding, physical, mechanical and acoustic properties of the tellurite glasses". *Radiation Effects and Defects in Solids*, **178**:1, 2022.

[17] E. Kavaz, H. O. Tekin, H. M. H. Zakaly, S. A. M. Issa, U. Kara, M. S. Al-Buriahi, S. Salah, K. A. Matori, and M. H. M. Zaid. "Structural and gamma-ray attenuation properties of different resin composites for radiation shielding applications". *Physics of Plasmas*, **52**:1, 2022.

[18] S. Issa, M. Sayyed, and M. Kurudirek. "Investigation of gamma radiation shielding properties of some zinc tellurite glasses". *Journal of Physical Science*, **27**:97, 2016.

[19] A. A. Ali, Y. S. Rammah, and M. H. Shaaban. "The influence of TiO2 on structural, physical and optical properties of B2O3 –TeO2 – Na2O – CaO glasses". *Journal of Non-Crystalline Solids*, **514**:52, 2019.

[20] S. H. Elazoumi, H. A. A. Sidek, Y. S. Rammah, R. El-Mallawany, M. K. Halimah, K. A. Matori, and M. H. M. Zaid. "Effect of PbO on optical properties of tellurite glass". *Results in Physics*, **8**:16, 2018.

[21] F. I. El-Agawany, E. Kavaz, U. Perişanoğlu, M. Al-Buriahi, and Y. S. Rammah. "Sm2O3 effects on mass stopping power/projected range and nuclear shielding characteristics of TeO2–ZnO glass systems". *Applied Physics A - Materials Science and Processing*, **125**:1, 2019.

[22] G. Kilic, E. Ilik, S. A. M. Issa, B. Issa, U. G. Issever, H. M. H. Zakaly, and H. O. Tekin. "Fabrication, structural, optical, physical and radiation shielding characterization of indium (III) oxide reinforced 85TeO2-(15–x)ZnO-xIn2O3 glass system". *Ceramics International*, **47**:27305, 2021.

[23] M. K. Halimah, A. A. Awshah, A. M. Hamza, K. T. Chan, S. A. Umar, and S. H. Alazoumi. "Effect of neodymium nanoparticles on optical properties of zinc tellurite glass system". *Journal of Materials Science: Materials in Electronics*, **31**:3785, 2020.

[24] I. O. Olarinoye, F. I. El-Agawany, A. El-Adawy, E. S. Yousef, and Y. S. Rammah. "Mechanical features, alpha particles, photon, proton, and neutron interaction parameters of TeO2–V2O3–MoO3 semiconductor glasses". *Ceramics International*, **46**:23134, 2020.

[25] N. Elkhoshkhany, R. El-Mallawany, and E. Syala. "Mechanical and thermal properties of TeO2–Bi2O3–V2O5–Na2O–TiO2 glass system". *Ceramics International*, **42**:19218, 2016.

[26] J. Kempe and A. Brahme. "Energy-range relation and mean energy variation in therapeutic particle beams". *Medical Physics*, **35**:159, 2008.

[27] W. Ulmer. "Theoretical aspects of energy–range relations, stopping power and energy straggling of protons". *Radiation Physics and Chemistry*, **76**:1089, 2007.

[28] J. F. Zieglera, M. D. Ziegler, and J. P. Biersack. "SRIM – The stopping and range of ions in matter (2010)". *Nuclear Instruments and Methods in Physics Research Section B: Beam Interactions with Materials and Atoms*, **268**:1818, 2010.

[29] L. Gerward, N. Guilbert, K. B. Jensen, and H. Levring. "WinXCom-a program for calculating X-ray attenuation coefficients". *Radiation Physics and Chemistry*, **71**:653, 2004.

[30] Y. S. Rammah, M. I. Sayyed, A. A. Ali, H. O. Tekin, and R. El-Mallawany. "Optical properties and gamma-shielding features of bismuth borate glasses". *Applied Physics A - Materials Science and Processing*, **124**:1, 2018.

[31] Özpolat-Ö.F.-Alım B. Sayyed M.I. Kurudirek M. Şakar, E. "Phy-X / PSD: Development of a user friendly online software for calculation of parameters relevant to radiation shielding and dosimetry". *Radiation Physics and Chemistry*, **166**:108496, 2020.

[32] M. L. Taylor, R. L. Smith, F. Dossing, and R. D. Franich. "Robust calculation of effective atomic numbers: The Auto- Z eff software". *Medical Physics*, **39**:1769, 2012.

[33] I. O. Olarinoye, R. I. Odiaga, and S. Paul. "EXABCal: A program for calculating photon exposure and energy absorption buildup factors". *Heliyon*, **5**:e02017, 2019.

[34] A. M. El-Khayatt. "Calculation of fast neutron removal cross-sections for some compounds and materials". *Annals of Nuclear Energy*, **37**:218, 2010.

[35] Y. S. Rammah, S. A. M. Issa, H. M. H. Zakaly, H. O. Tekin, E. Yousef, and A. S. Abouhaswa. "B2O3-Bi2O3-Li2O3-Cr2O3 glasses: fabrication, structure, mechanical, and gamma radiation shielding qualities". *Journal of the Australian Ceramic Society*, **57**:1057, 2021.

[36] V. P. Singh and N. M. Badiger. "A comprehensive study on gamma-ray exposure build-up factors and fast neutron removal cross sections of fly-ash bricks". *Journal of Ceramics*, **2013**:1, 2013.

[37] J. H. Hubbell. "Photon mass attenuation and energy-absorption coefficients". *The International Journal of Applied Radiation and Isotopes*, **33**:1269, 1982.

[38] H. O. Tekin, S. A. M. Issa, E. M. Ahmed, and Y. S. Rammah. "Lithium-fluoro borotellurite glasses: Nonlinear optical, mechanical characteristics and gamma radiation protection characteristics". *Radiation Physics and Chemistry*, **190**:109819, 2022.

[39] Y. S. Rammah, F. I. El-Agawany, E. A. A. Wahab, M. M. Hessien, and K. S. Shaaban. "Significant impact of V2O5 content on lead phosphor-arsenate glasses for mechanical and radiation shielding applications". *Radiation Physics and Chemistry*, **193**:109956, 2022.

[40] M. Zhukovsky, M. S. I. Koubisy, H. M. H. Zakaly, A. S. Ali, S. A. M. Issa, and H. O. Tekin. "Dielectric, structural, optical and radiation shielding properties of newly synthesized CaO–SiO2–Na2O–Al2O3 glasses: experimental and theoretical investigations on impact of Tungsten(III) oxide". *Applied Physics A - Materials Science and Processing*, **128**:1, 2022.